# Coexisting mechanisms of thermally driven magnetization reversal in shakti spin ice systems

Vladyslav M. Kuchkin [1,*] Unnar B. Arnalds [2] Hannes Jónsson [2] and Pavel F. Bessarab [2,3,†]
[1]Department of Physics and Materials Science, University of Luxembourg, L-1511 Luxembourg, Luxembourg
[2]Science Institute and Faculty of Physical Sciences, University of Iceland, 107 Reykjavík, Iceland
[3]Department of Physics and Electrical Engineering, Linnaeus University, SE-39231 Kalmar, Sweden

(Received 5 March 2025; accepted 17 August 2025; published 2 September 2025)

The switching mechanisms in artificial spin ice systems are investigated with focus on shakti and vertex-modified shakti lattices. Minimum energy paths are calculated using the geodesic nudged elastic band method implemented with a micromagnetic description of the system, including the internal magnetic structure of the islands and edge deviations. Two switching mechanisms, uniform magnetization rotation and domain wall formation, are found to have comparable activation energies. The preference for one over the other depends strongly on the saturation magnetization and the magnetic ordering of neighboring islands. Surprisingly, these mechanisms can coexist, leading to an enhanced probability of magnetization reversal. These results provide valuable insight that can help control internal magnetization switching processes in spin ice systems and help predict their thermodynamic properties.

DOI: 10.1103/pr2y-dfbd

## I. INTRODUCTION

Artificial spin ice (ASI) systems [1–5] represent interacting nanomagnets demonstrating complex emergent behaviors arising from geometrically imposed frustration. Unlike naturally occurring frustrated magnets, ASI offers precise control over lattice geometry and interaction patterns, enabling systematic studies of frustration and collective dynamics. Due to their unique magnetic properties, spin ice systems have potential for various applications in next-generation data storage devices [6], neuromorphic computations [7,8], and quantum computing [9]. Magnetic ordering and dynamics observed in artificial spin ice systems have been a rich playground for investigations of a multitude of phenomena in interacting nanomagnetic systems of different geometries [10–13]. Such systems have been used for investigating ordering in frustrated systems [12,14–16] and higher-order vertex interactions and how they are modified by the geometry of the islands [17] as well as spin wave dynamics both internally in the islands and between islands [18–20].

Several articles have dealt with the thermal dynamics involved in artificial spin ice systems, e.g., as the systems transition from a frozen ordered state to a thermally active state or can be thermally activated by heating to an elevated temperature [21,22]. These dynamics arise from thermally activated reversals of the magnetization of individual islands from the two opposing energy-minimum states.

These studies highlight the importance of the energy barrier on the ordering in the system as any potential dynamics in these systems are directly coupled to the reversal mechanism and energy barrier of individual islands. This important role is, e.g., exemplified in shakti [Figs. 1(a) and 1(b)] and Saint George spin ice lattices composed of islands with different reversal energy barriers, which freeze into a low-temperature state at different temperatures governed by their reversal barrier and the magnetic arrangement of their neighboring islands [23–25]. For the chosen two building block geometries, we achieved quite similar but still striking results of the coexistence of different switching mechanisms. So, one can expect similar effects in ASI systems of other geometries once a more advanced analysis based on micromagnetic theory is conducted.

In many cases, simple models can be employed to determine the energy barrier for an island reversal, such as determining them directly using the Stoner-Wolfarth model for ellipsoidal islands [26] as well as micromagnetic modeling of the energy barrier, assuming uniform rotation of magnetization. These model calculations are, however, limited as they do not capture thermal effects and exclude nonuniform magnetization reversal mechanisms from consideration. Such calculations may also neglect any potential deviations in the magnetization direction occurring at the edges of the islands arising from interactions with neighboring islands at the vertex and how they potentially alter the magnetization switching between the two ground states. In addition to the reversal barrier inherent in individual islands, the vertex arrangements of islands have recently been shown to comprise an additional modification of the energy landscape within individual islands through edge magnetization deviations at the ends of the

*Contact author: vladyslav.kuchkin@uni.lu
†Contact author: pavel.bessarab@lnu.se

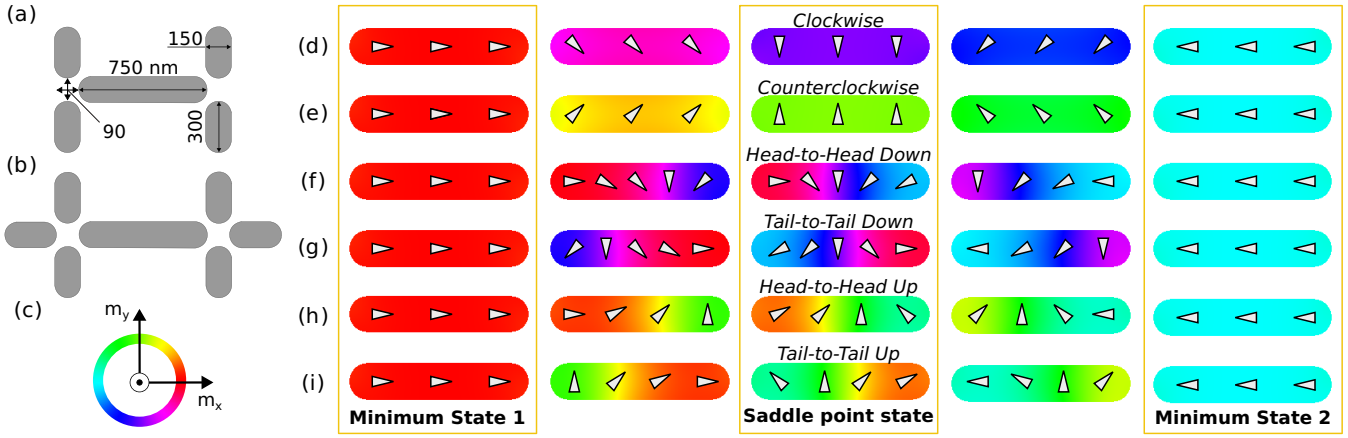


FIG. 1. Island magnetization reversal mechanisms. (a), (b) The arrangements of the shakti lattice building block and the vertex-modified shakti geometry used for the calculations of the reversal barrier for long islands. The color code used to indicate the magnetization direction is illustrated in panel (c). (d)–(i) The six possible switching mechanisms of the long island: uniform rotation (clockwise and counterclockwise) and domain wall formation with head-to-head and tail-to-tail types, with down ($-\boldsymbol{e}_y$) and up ($+\boldsymbol{e}_y$) directions of the central spin.

islands, rich in dynamics and adding to the ordering phenomena of ASI systems [18,27,28].

In this study, we develop and apply micromagnetic-based minimum energy path (MEP) calculations to determine energy barriers in square and shakti artificial spin ice. Using our model, we obtain full energy barrier profiles and intermediate states of the systems as they traverse between energy-minimum states. Determining the reversal energy barrier for individual islands as a function of island magnetization, we observe a crossover between the reversal mechanisms from a uniform rotation to a domain wall formation. Above this bifurcation point, our modeling shows both the reversal mechanisms to be stabilized, enabling the reversal to occur through two pathways, potentially affecting the dynamics of the system, especially close to the bifurcation point. Altering the magnetization of neighboring islands we observe the reversal mechanism to be strongly affected by the magnetization direction of neighboring islands.

## II. MODEL AND METHOD

The Hamiltonian used for describing spin ice systems is of the following form:

$$\mathcal{H} = l \int \left( \mathcal{A}[(\partial_x \boldsymbol{m})^2 + (\partial_y \boldsymbol{m})^2] - \frac{1}{2} M_s \boldsymbol{b}_d \cdot \boldsymbol{m} \right) dS, \qquad (1)$$

where $\boldsymbol{m}$ is the unit vector in the direction of local magnetization, $\mathcal{A}$ is the exchange stiffness constant, $M_s$ is the saturation magnetization, $\boldsymbol{b}_d$ is the demagnetizing field, $l$ is the thickness of the islands, and $dS = dxdy$ is the area element of the islands. We fix $l = 3.3$ nm to be much smaller than the island width and thus can neglect magnetization variation along the island thickness, i.e., $\boldsymbol{m} = \boldsymbol{m}(x, y)$. The exchange constant equals 13 pJ/m, which is a standard value for permalloy [29]. We vary the saturation magnetization value in the range [100, 350] kA/m in most simulations, and only for calculating energy barriers and reversals for edge modulation states, we consider $M_s = 800$ kA/m. Several materials have been shown to have a tunable magnetization within this range. Among these materials are amorphous alloys of CoAlZr, where the magnetization and Curie temperature can be tuned via Co concentration in a large range [30,31]. The geometry of the spin ice system we investigate is shown in Fig. 1. For investigating the magnetization reversal barrier and mechanism of the long islands, we focus our attention on the building block of the shakti geometry shown in Fig. 1(a), where two small islands are connected to the long island vertex [23,25]. Additionally, we explore a vertex-modified shakti geometry shown in Fig. 1(b), where an additional third small island is connected to the long island vertex. Such vertices occur in the staggered shakti geometry, which is composed of both types of long island vertices explored in this work [12]. For both cases, we focus our study on the switching of the long island, while the smaller islands remain in their primary magnetization. We use a standard color code [Fig. 1(c)] to visualize the magnetization within the islands.

To obtain equilibrium states in the spin ice systems, we minimize the energy given by Eq. (1) in the Mumax3 software [29] relying on the steepest descent methods, i.e., utilizing the effective field $\boldsymbol{B}_{\text{eff}} = -M_s^{-1} \delta\mathcal{H}/\delta\boldsymbol{m}$. Calculation of MEPs and energy barriers between any two stable states is done with the geodesic nudged elastic band (GNEB) method [32,33], which is implemented in Mumax3 and available in a GitHub repository [34]. Recently performed GNEB calculations for complex magnetic spin textures such as skyrmions [35,36], hopfions [37,38], and magnetic bubbles [39] in multilayer systems demonstrate its high efficiency in studying a wide variety of textures. According to the method, we consider a set of $N$ states, referred to as images, $\boldsymbol{M}_\nu$, where the initial $\nu = 1$ and final $\nu = N$ images correspond to equilibrium points, while all intermediate $1 < \nu < N$ images are movable points. Each of the movable images, $\boldsymbol{M}_\nu$, is subject to a force $\boldsymbol{F}_\nu$ arising from the effective field $\boldsymbol{B}_{\text{eff}}$ and from adjacent images $\boldsymbol{M}_{\nu-1}$ and $\boldsymbol{M}_{\nu+1}$. The latter force is a spring force and is proportional to the geodesic distance between images. Applying the velocity projection optimization method, the forces $\boldsymbol{F}_\nu$ are zeroed to a given tolerance. In the Mumax3 code, we have simulated 15 images interacting through the forces $\boldsymbol{F}_\nu$. All derivatives in Eq. (1) are approximated with the second-order finite difference scheme.

The GNEB method makes it possible to determine MEPs between magnetic states, thereby revealing the transition mechanisms. The point of highest energy along an MEP corresponds to the saddle point on the energy surface of the system, which defines the energy barrier and the rate of transition within the harmonic approximation to the transition state theory [40,41]. The GNEB method thus provides a practical framework for analyzing the thermal stability of magnetic states, especially in regimes where the thermal energy is much smaller than the energy barrier. In such cases, thermally activated transitions become rare events on the timescale of precessional dynamics, making direct simulations of magnetization dynamics via numerical integration of the stochastic Landau-Lifshitz-Gilbert equation computationally impractical for calculating transition rates. At moderate temperatures, where transitions occur more frequently, direct comparisons between GNEB-based predictions and magnetization dynamics simulations become feasible. Such comparisons have been performed in previous studies [36,37,40,42], showing good agreement between the two approaches.

While the energy barriers obtained from the GNEB calculations are the primary quantities determining the thermal stability of magnetic states, calculating transition rates and lifetimes also requires an evaluation of the Arrhenius preexponential factor [40,41]. A detailed analysis of these rates and lifetimes lies beyond the scope of the present work and will be addressed in future research.

## III. RESULTS

### A. Saddle points

Every island in the spin ice system is magnetized along the primary axis due to the shape anisotropy. As shown in Fig. 1, switching between right- and left-magnetized islands, denoted as Minimum States 1 and 2, can occur via uniform rotation [Figs. 1(d) and 1(e)] or via domain wall formation [Figs. 1(f)–1(i)] represented by the saddle point configurations and illustrated in the figure. Here, we ignore multidomain switching mechanisms [43] as they have higher energy barriers in the range of saturation magnetization values we consider and are only relevant in the case of high $M_s$. In the case of planar magnets, the characteristic size of the domain wall is given by the exchange length $l_{\mathrm{ex}} = \sqrt{2\mathcal{A}/(\mu_0 M_s^2)}$, which can be used as a good estimate for comparing the domain wall width to the size of the islands. For the values of $M_s$ considered in this study, $l_{\mathrm{ex}}$ lies in the range 15–45 nm.

For a single island switching, clockwise (CW) and counterclockwise (CCW) uniform rotations [Figs. 1(d) and 1(e)] have identical energy barriers due to the symmetry of the system. The same holds for four types of switching via the domain wall formation [Figs. 1(f)–1(i)]. However, in spin ice systems, the way neighboring islands are magnetized will differentiate these switching cases. Due to the presence of the small islands, energy barriers for CW and CCW switchings do not generally coincide. The same holds for the domain wall formation mechanisms. We distinguish four types of domain wall transitions: head-to-head down (HHD), tail-to-tail down (TTD), head-to-head up (HHU), and tail-to-tail up (TTU) shown in Figs. 1(f)–1(i).

### B. Shakti geometry

Considering the symmetry of the shakti building block geometry, there are five unique cases for the magnetic arrangement of the surrounding small islands when considering the energy and reversal of the long island. An overview of energetically representative states is shown in Figs. 2(a)–2(e). Each of those energetically identical cases has its own symmetry, which is reflected in the switching mechanisms and nonequivalence of the MEPs. The general feature of all MEPs is that uniform rotation switching (CW and CCW) appears only at low saturation magnetization values, while switching via domain wall formation (HHD, TTD, HHU, and TTU) is present at higher values of $M_s$. However, at some intermediate values of $M_s$, all types of reversal mechanisms can coexist depending on the magnetization of the neighboring islands and their symmetry. Note that in a generic model of a bistable magnet characterized by exchange and anisotropy, uniform rotation of magnetization cannot coexist with other reversal modes (see Appendix A). Therefore, the coexistence of switching mechanisms arises from magnetostatic interactions beyond shape anisotropy, as well as the influence of neighboring islands. Geometries based on islands of differing length, such as the shakti lattice, constitute systems with an engineered energy hierarchy, with the long islands having a higher blocking temperature than the small islands. At the temperature at which magnetization reversal takes place for the long islands, the small islands are thermally active and rapidly switching between their two low energy states. The magnetostatic coupling between the elements still has a direct impact on the activation energy of each island. The instantaneous magnetic orientations of the small islands therefore affects the reversal barrier and reversal mechanism of the long islands.

The configurations shown in Figs. 2(a) and 2(e) are characterized by the lowest symmetry. This results in that CW and CCW switchings have different energy barriers; in other words, their MEPs are not equivalent. Different energy barriers are also observed for switching via domain wall formation. In the case shown in Fig. 2(a), energy profiles along MEPs for HHD (HHU) and TTD (TTU) coincide, but a minor splitting is observed for HHD and HHU, while for the case shown in Fig. 2(e), all MEPs correspond to different energy barriers. Configurations shown in Figs. 2(b)–2(d) are more symmetric and MEPs for CW and CCW transitions are equivalent. For cases shown in Figs. 2(b) and 2(c), all switching mechanisms involving domain wall formation are equivalent. However, the head-to-head and tail-to-tail domain wall switching mechanisms are not equivalent for the case shown in Fig. 2(d). Additionally, at $M_s = 200$ kA/m, CW and CCW transitions are present only for geometries (a)–(c). Reversal mechanism simulations for the vertex-modified shakti geometry revealed similar results to those for the shakti geometry, with both uniform rotation and domain wall reversal mechanisms present. The resulting energy barriers for varying magnetization are provided in Appendix B. In both shakti and vertex-modified shakti systems, the energy barriers are on the order of 0.1–1 eV, which is larger than 25 meV—the thermal energy available at room temperature. However, assuming a reasonable attempt frequency, we can expect thermally

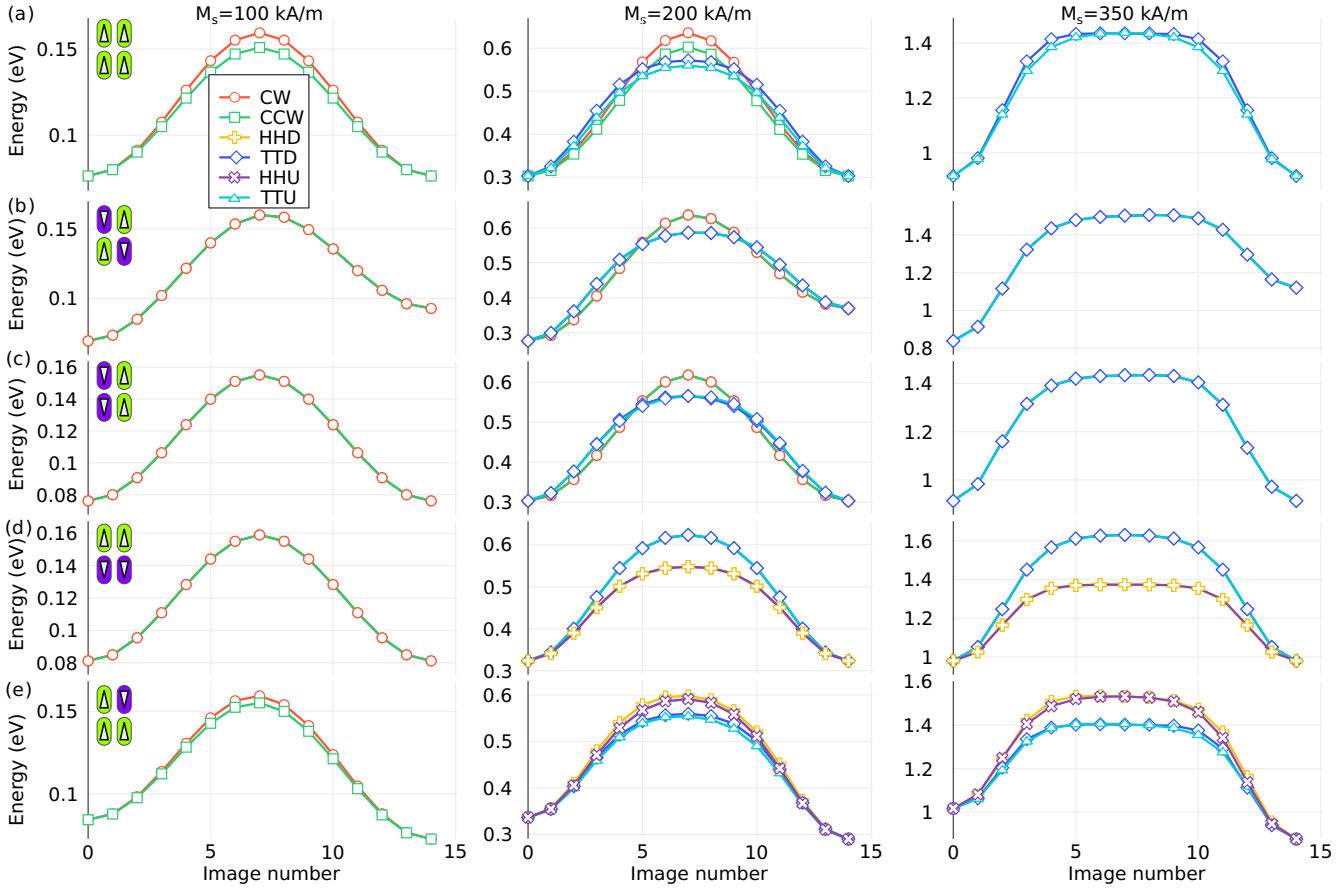


FIG. 2. Switching mechanisms in the shakti system. (a)–(e) MEPs for five cases for different magnetizations of the small islands and values of $M_s = 100$, 200, and 350 kA/m. The orientation of the four small islands, surrounding the long island, is given in the top-left insets. CW and CCW switchings are present only for $M_s = 100$ kA/m [panels (a)–(e)] and for $M_s = 200$ kA/m [panels (a)–(c)]. HHD, TTD, HHU, and TTU switchings are present for $M_s = 200$ kA/m and $M_s = 350$ kA/m. In cases (a)–(c), MEPs for HHD (HHU) coincide with those for TTD (TTU), while for geometries (d) and (e), MEPs for HHD (TTD) are comparable to HHU (TTU).

excited reversal to occur within a reasonable timescale, even at room temperature.

In the theory of magnetization reversal, transitions with the lowest energy barrier are typically of primary interest. By comparing the cases shown in Fig. 2, it becomes evident that uniform rotation and switching via domain wall can both represent the primary switching mechanism at different $M_s$. Consequently, the coexistence of different switching mechanisms can be anticipated at a specific magnetization saturation. In the following, we explore this in more detail.

### C. Primary switching mechanisms

As illustrated in the discussion above, the GNEB method reveals different switching mechanisms for the long island in a shakti geometry depending on the saturation magnetization value and the arrangement of neighboring islands. To investigate the reversal mechanism and its evolution systematically, we performed multiple runs of GNEB simulations for different values of $M_s$ and compared energy barriers for uniform reversal switching and switching via domain wall reversal. Graphs summarizing the results are shown in Fig. 3. For states shown in Fig. 3(a), uniform rotation is the only mechanism for $M_s < 160$ kA/m, and switching through the domain wall formation is not present. For $M_s > 160$ kA/m, the simulations revealed two mechanisms to be stable: uniform rotation and switching through domain wall formation with a lower energy. For the states shown in Fig. 3(b), there is no such strict distinction, and for the intermediate value of $M_s$, the saddle point rather represents a combination of a uniform rotation state and domain wall reversal. The corresponding saddle point configurations are provided in Fig. 3(b).

### D. Edge deviations

To better understand the effect of neighboring islands on the reversal mechanism, we investigated edge deviations in so-called type I and type IV vertex states in artificial square spin ice vertices shown in Fig. 4. These states have been shown to have antiparallel [Fig. 4(a)] and flux-closure [Fig. 4(b)] edge deviations [18,27,28]. In each case, the symmetric edge modulation states are separated by energy barriers, which can be identified by the GNEB method. As we can deduce from Fig. 4(c), these barriers are substantially smaller in magnitude than those discussed previously, and in order to observe them, higher values of saturation magnetization are needed, so

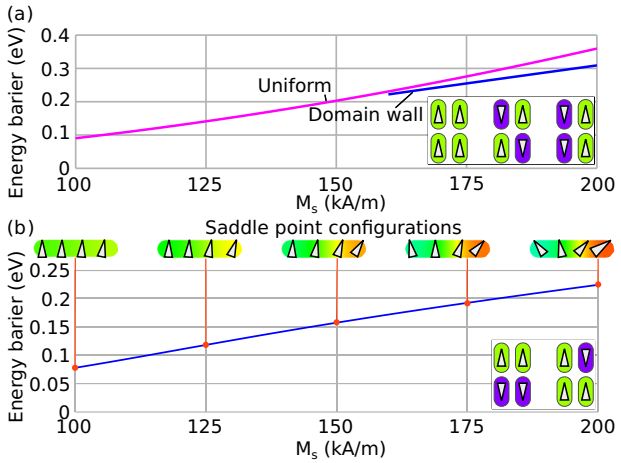


FIG. 3. Primary mechanism for magnetization reversal. (a), (b) The calculated energy barriers for the magnetization reversal of the long islands as a function of saturation magnetization. Panels (a) and (b) correspond to different magnetization directions of the four neighboring small islands, as schematically illustrated in the bottom-right insets. In the cases shown in panel (a), there are two mechanisms—uniform rotation and switching via the domain wall formation—that have a crossing point at $M_s \simeq 160$ kA/m. In the cases shown in panel (b), there is only one primary switching mechanism representing a mixture of those two. The inset images above panel (b) show saddle point states for selected values of $M_s$.

we utilize $M_s = 800$ kA/m for simulations. Thus, we do not expect a significant influence of such edge deviations on the energy barrier magnitude for $M_s \in [100, 350]$ kA/m, as discussed above. However, these edge deviations will affect the reversal pathway, i.e., whether the reversal occurs through a CW or CCW reversal for uniform rotation or via HHU, HHD, TTU, or TTD reversal for domain wall formation. At higher values of $M_s$, when the edge deviations can be observed, one has to take into account more diverse possibilities for saddle point configurations, e.g., states with multiple domain walls, vortices, etc., especially for long islands. Analysis of such transitions is beyond the scope of the current work and will be the subject of further investigation.

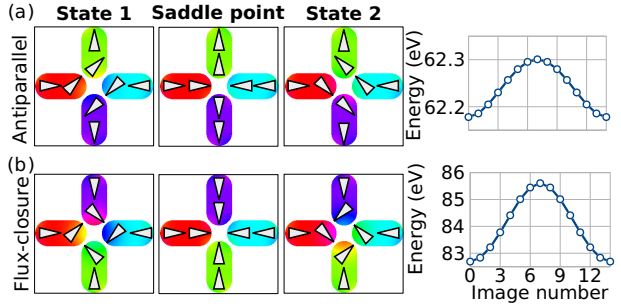


FIG. 4. Edge deviations. (a), (b) Spin textures corresponding to the antiparallel and flux-closure edge deviations, respectively. The MEPs calculated for $M_s = 800\,\mathrm{kA/m}$. The antiparallel states are separated by an energy barrier of $\Delta E = 0.1\,\mathrm{eV}$, while the flux-closure edge deviation states are separated by a barrier of $\Delta E = 2.9\,\mathrm{eV}$.

## IV. CONCLUSIONS

In conclusion, we study the switching mechanisms of shakti spin ice and vertex-modified shakti geometries using the geodesic nudged elastic band method implemented in combination with a micromagnetic description of the system. Our findings reveal two reversal mechanisms—uniform rotation and switching via domain wall formation. The corresponding energy barriers depend on the material's saturation magnetization and on the magnetization arrangement of neighboring islands. Critical values for $M_s$ have been identified at which a change in the primary reversal mechanism occurs, resulting in a bifurcation point of coexisting reversal mechanisms. Finally, the role of low-energy barriers corresponding to edge deviations in the modification of these primary mechanisms is revealed. The reversal pathways are found to be modified by the magnetic arrangement of neighboring islands, and this is particularly important to take into account for materials with high $M_s$. In such cases, there can even be the possibility of switching mechanisms via multidomain wall formation.

## ACKNOWLEDGMENTS

V.M.K. acknowledges financial support from the National Research Fund of Luxembourg under the CORE Grant No. C22/MS/17415246/DeQuSky and from the European Union's Horizon 2020 Research and Innovation Programme under the Marie Skłodowska-Curie Grant Agreement No. 101203692 (QUANTHOPF). This work was supported by funding for the project Magnetic Metamaterials from the Icelandic Research Fund (Grant No. 2410333), by the University of Iceland Research Fund, by the Swedish Research Council (Grant No. 2020-05110), and by the Crafoord Foundation (Grant No. 20231063). The authors acknowledge Hendrik Schrautzer, Moritz Sallermann, Jan Masell, and Jonathan Leliaert for valuable discussions.

## DATA AVAILABILITY

The data that support the findings of this article are not publicly available upon publication because it is not technically feasible and/or the cost of preparing, depositing, and hosting the data would be prohibitive within the terms of this research project. The data are available from the authors upon reasonable request.

## APPENDIX A: CROSSOVER BETWEEN SWITCHING MECHANISMS IN A UNIAXIAL MAGNET

We consider a one-dimensional model of a ferromagnet equipped with the uniaxial anisotropy along the system's axis. The energy of the system reads

$$E = \int_0^L \left[ A\left(\frac{d\boldsymbol{m}}{dx}\right)^2 - K m_x^2 \right] dx, \tag{A1}$$

where $L$ is the system size and $K > 0$ is an easy-axis anisotropy constant. There are two stable states with $\boldsymbol{m}$ pointing either along or opposite to the $x$ axis. In the macrospin approximation, there is only one (degenerate) saddle point

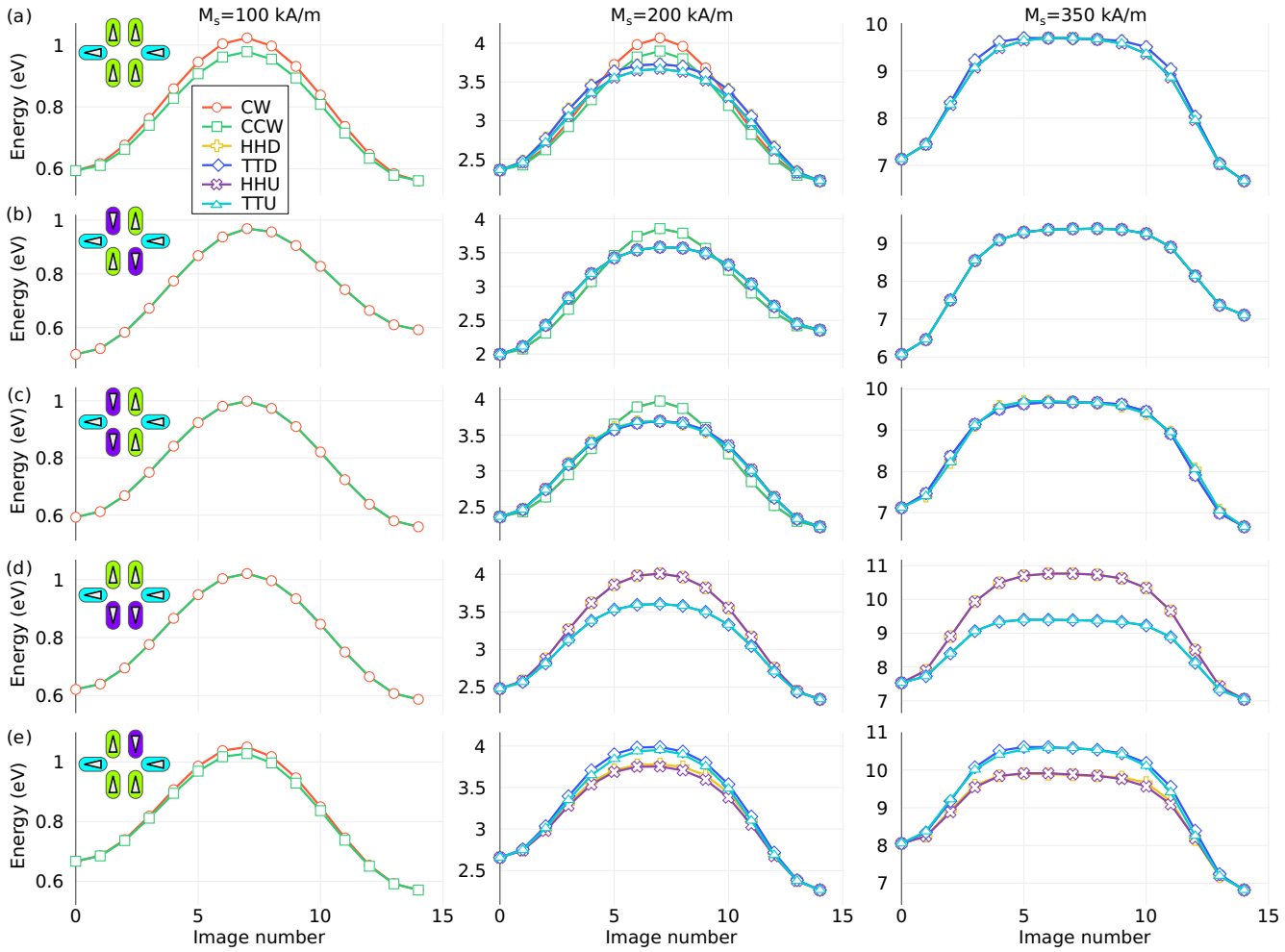


FIG. 5. Switching mechanisms in the vertex-modified shakti system: type 1. (a)–(e) MEPs for five cases for different magnetizations of the small islands and values of $M_s = 100$, 200, and 350 kA/m. The orientation of the six neighboring small islands is given in the top-left insets. CW and CCW switchings are present only for $M_s = 100$ kA/m [panels (a)–(e)] and for $M_s = 200$ kA/m [panels (a)–(c)]. HHD, TTD, HHU, and TTU switchings are present for $M_s = 200$ kA/m and $M_s = 350$ kA/m. In cases (a)–(c), MEPs for HHD (HHU) coincide with those for TTD (TTU), while for geometries (d) and (e), MEPs for HHD (TTD) are comparable to HHU (TTU).

corresponding to $\boldsymbol{m}$ orthogonal to the $x$ axis. The task is to identify under what conditions this state is a saddle point of the functional given by Eq. (A1). Rewriting the functional in terms of the spherical coordinates $\boldsymbol{m} = (\sin\theta\cos\varphi, \sin\theta\sin\varphi, \cos\theta)$ and expanding it around the the point $\theta_0 = \pi/2, \varphi_0 = \pi/2$ to the second order of the deviation yields

$$E \approx E_0 + \int_0^L \boldsymbol{\xi}^T D\boldsymbol{\xi} dx, \tag{A2}$$

where $E_0 = 0$ is the energy of the collinear state with $\boldsymbol{m}(x)$ perpendicular to the $x$ axis, $\boldsymbol{\xi}^T = [\delta\theta(x), \delta\varphi(x)]$ describes the deviation, and the operator $D$ is given by the following equation:

$$D \equiv \begin{pmatrix} -A\dfrac{d^2}{dx^2} & 0 \\ 0 & -A\dfrac{d^2}{dx^2} - K \end{pmatrix}. \tag{A3}$$

The eigenvalues of $D$ are fixed by the boundary condition $\boldsymbol{\xi}(0) = \boldsymbol{\xi}(L) = 0$:

$$\varepsilon_n^{\pm} = \frac{A\pi^2 n^2}{L^2} - \frac{1}{2}(K \pm K), \tag{A4}$$

where $n$ is an integer number. There is at least one zero eigenvalue $\varepsilon_0^- = 0$ that corresponds to the zero mode—rotation of the magnetization around the $x$ axis. There is at least one negative eigenvalue, $\varepsilon_0^+ = -K$. If this is the only negative eigenvalue, the collinear state corresponds to a degenerate first-order saddle point and a true mechanism of magnetization reversal. This is the case when $\varepsilon_1^{(+)} = A\pi^2/L^2 - K > 0$, which is realized when $L < L_0$, with $L_0$ being the domain wall width: $L_0 = \pi\sqrt{A/K}$. However, the second eigenvalue becomes negative when $L > L_0$. This indicates a crossover between the mechanisms of the reversal: The collinear rotation breaks down, and nonuniform rotation of magnetization is established.

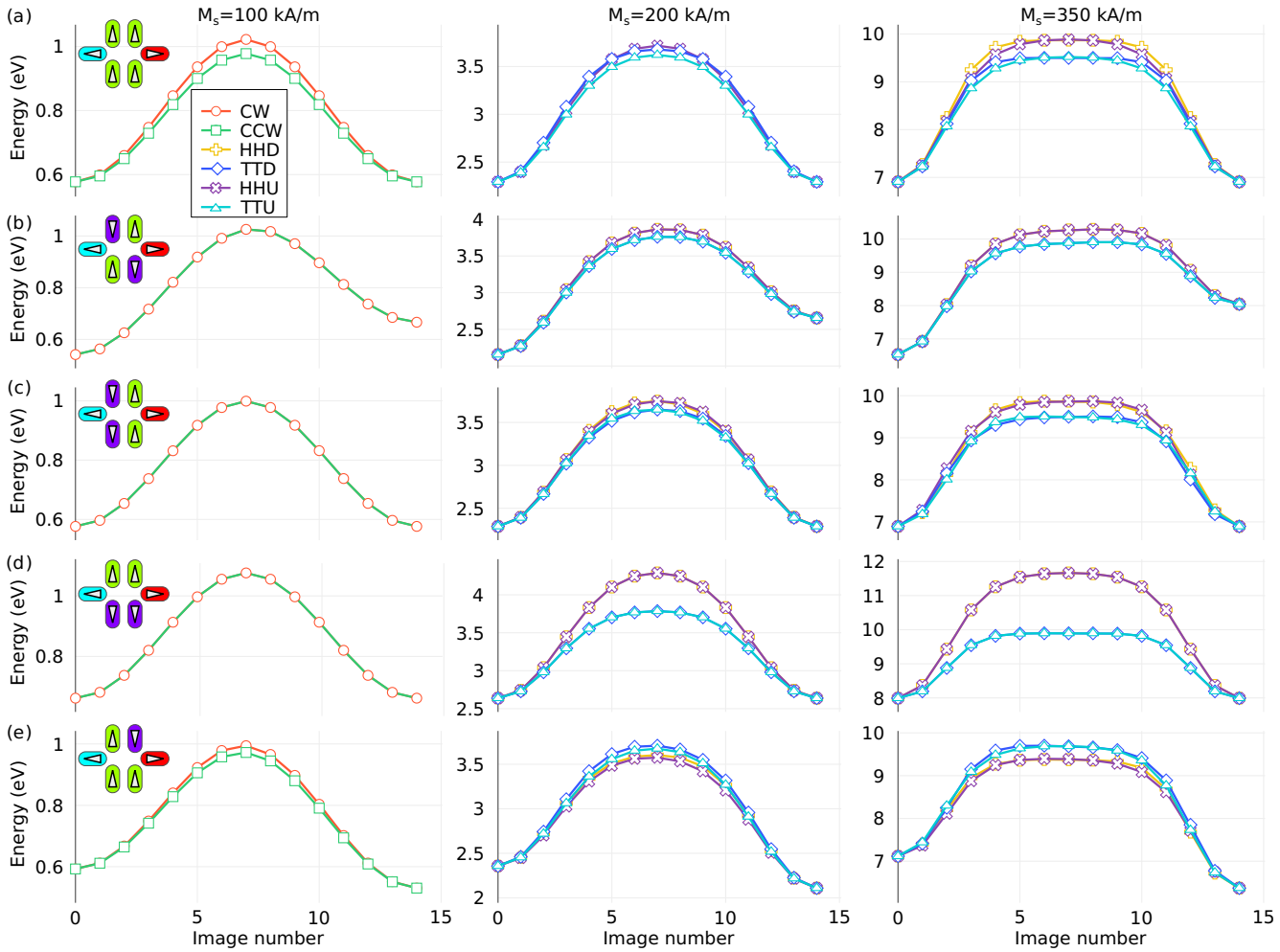


FIG. 6. Switching mechanisms in the vertex-modified shakti system: type 2. (a)–(e) MEPs for five cases for different magnetizations of the small islands and values of $M_s = 100$, 200, and 350 kA/m. The orientation of the six neighboring small islands is given in the top-left insets. CW and CCW switchings are present only for $M_s = 100$ kA/m. HHD, TTD, HHU, and TTU switchings are present for $M_s = 200$ kA/m and $M_s = 350$ kA/m. In cases (a)–(c), MEPs for HHD (HHU) coincide with those for TTD (TTU), while for geometries (d) and (e), MEPs for HHD (TTD) are comparable to HHU (TTU).

## APPENDIX B: SWITCHING MECHANISMS IN VERTEX-MODIFIED SHAKTI SPIN ICE SYSTEMS

Performing GNEB simulations for the vertex-modified shakti geometry, we obtain magnetization reversal mechanisms similar to the case of the shakti geometry. In addition to the five orientations of the small vertical islands, we must consider two types of lateral island magnetizations. We refer to cases in which the lateral islands are identically or oppositely magnetized as type 1 and type 2, respectively. The results of simulations of type 1 vertex-modified shakti geometry are shown in Fig. 5 and qualitatively are similar to the case of the shakti geometry discussed in the main text. The main difference we can point out here is the energy difference between the initial and final states, which arises from the interaction of the long island with the additional lateral islands. The results of simulations of type 2 vertex-modified shakti geometry are shown in Fig. 6. The significant difference between this case and the shakti geometry is the absence of uniform rotation switching at $M_s = 200$ kA/m for all types of island orientations [Figs. 6(a)–6(e)]. This indicates that the primary switching mechanism changes at lower values of $M_s$ compared to results shown in Fig. 3.

[1] R. F. Wang, C. Nisoli, R. S. Freitas, J. Li, W. McConville, B. J. Cooley, M. S. Lund, N. Samarth, C. Leighton, V. H. Crespi, and P. Schiffer, Artificial 'spin ice' in a geometrically frustrated lattice of nanoscale ferromagnetic islands, Nature (London) **439**, 303 (2006).

[2] L. J. Heyderman and R. L. Stamps, Artificial ferroic systems: Novel functionality from structure, interactions and dynamics, J. Phys.: Condens. Matter **25**, 363201 (2013).

[3] I. Gilbert, C. Nisoli, and P. Schiffer, Frustration by design, Phys. Today **69**, 54 (2016).

[4] C. Nisoli, V. Kapaklis, and P. Schiffer, Deliberate exotic magnetism via frustration and topology, Nat. Phys. **13**, 200 (2017).

[5] C. Rodríguez-Gallo, A. Ortiz-Ambriz, C. Nisoli, and P. Tierno, Geometrical control of topological charge transfer in shakti-Cairo colloidal ice, Commun. Phys. **6**, 113 (2023).

[6] P. Schiffer and C. Nisoli, Artificial spin ice: Paths forward, Appl. Phys. Lett. **118**, 110501 (2021).

[7] J. C. Gartside, K. D. Stenning, A. Vanstone, H. H. Holder, D. M. Arroo, T. Dion, F. Caravelli, H. Kurebayashi, and W. R. Branford, Reconfigurable training and reservoir computing in an artificial spin-vortex ice via spin-wave fingerprinting, Nat. Nanotechnol. **17**, 460 (2022).

[8] W. Hu, Z. Zhang, Y. Liao, Q. Li, Y. Shi, H. Zhang, X. Zhang, C. Niu, Y. Wu, W. Yu, X. Zhou, H. Guo, W. Wang, J. Xiao, L. Yin, Q. Liu, and J. Shen, Distinguishing artificial spin ice states using magnetoresistance effect for neuromorphic computing, Nat. Commun. **14**, 2562 (2023).

[9] A. D. King, C. Nisoli, E. D. Dahl, G. Poulin-Lamarre, and A. Lopez-Bezanilla, Qubit spin ice, Science **373**, 576 (2021).

[10] S. H. Skjærvø, C. H. Marrows, R. L. Stamps, and L. J. Heyderman, Advances in artificial spin ice, Nat. Rev. Phys. **2**, 13 (2020).

[11] E. Östman, H. Stopfel, I.-A. Chioar, U. B. Arnalds, A. Stein, V. Kapaklis, and B. Hjörvarsson, Interaction modifiers in artificial spin ices, Nat. Phys. **14**, 375 (2018).

[12] M. J. Morrison, T. R. Nelson, and C. Nisoli, Unhappy vertices in artificial spin ice: New degeneracies from vertex frustration, New J. Phys. **15**, 045009 (2013).

[13] U. B. Arnalds, J. Chico, H. Stopfel, V. Kapaklis, O. Bärenbold, M. A. Verschuuren, U. Wolff, V. Neu, A. Bergman, and B. Hjörvarsson, A new look on the two-dimensional Ising model: Thermal artificial spins, New J. Phys. **18**, 023008 (2016).

[14] G.-W. Chern, M. J. Morrison, and C. Nisoli, Degeneracy and criticality from emergent frustration in artificial spin ice, Phys. Rev. Lett. **111**, 177201 (2013).

[15] I. Gilbert, Y. Lao, I. Carrasquillo, L. O'Brien, J. D. Watts, M. Manno, C. Leighton, A. Scholl, C. Nisoli, and P. Schiffer, Emergent reduced dimensionality by vertex frustration in artificial spin ice, Nat. Phys. **12**, 162 (2016).

[16] J. Drisko, T. Marsh, and J. Cumings, Topological frustration of artificial spin ice, Nat. Commun. **8**, 14009 (2017).

[17] N. Strandqvist, G. Fitez, O. Heinonen, and P. Schiffer, Nanomagnet shape effects on magnetic reversal in artificial spin ice, Phys. Rev. B **111**, 184420 (2025).

[18] B. E. Skovdal, S. D. Slöetjes, M. Pohlit, H. Stopfel, V. Kapaklis, and B. Hjörvarsson, Thermal excitations within and among mesospins in artificial spin ice, Phys. Rev. B **107**, L060406 (2023).

[19] D. M. Arroo, J. C. Gartside, and W. R. Branford, Sculpting the spin-wave response of artificial spin ice via microstate selection, Phys. Rev. B **100**, 214425 (2019).

[20] J. C. Gartside, A. Vanstone, T. Dion, K. D. Stenning, D. M. Arroo, H. Kurebayashi, and W. R. Branford, Reconfigurable magnonic mode-hybridisation and spectral control in a bicomponent artificial spin ice, Nat. Commun. **12**, 2488 (2021).

[21] U. B. Arnalds, A. Farhan, R. V. Chopdekar, V. Kapaklis, A. Balan, E. T. Papaioannou, M. Ahlberg, F. Nolting, L. J. Heyderman, and B. Hjörvarsson, Thermalized ground state of artificial kagome spin ice building blocks, Appl. Phys. Lett. **101**, 112404 (2012).

[22] V. Kapaklis, U. B. Arnalds, A. Farhan, R. V. Chopdekar, A. Balan, A. Scholl, L. J. Heyderman, and B. Hjörvarsson, Thermal fluctuations in artificial spin ice, Nat. Nanotechnol. **9**, 514 (2014).

[23] H. Stopfel, E. Östman, I.-A. Chioar, D. Greving, U. B. Arnalds, T. P. A. Hase, A. Stein, B. Hjörvarsson, and V. Kapaklis, Magnetic order and energy-scale hierarchy in artificial spin-ice structures, Phys. Rev. B **98**, 014435 (2018).

[24] H. Stopfel, U. B. Arnalds, A. Stein, T. P. A. Hase, B. Hjörvarsson, and V. Kapaklis, Multiple energy scales in mesospin systems: The vertex-frustrated Saint George lattice, Phys. Rev. Mater. **5**, 114410 (2021).

[25] I. Gilbert, G.-W. Chern, S. Zhang, L. O'Brien, B. Fore, C. Nisoli, and P. Schiffer, Emergent ice rule and magnetic charge screening from vertex frustration in artificial spin ice, Nat. Phys. **10**, 670 (2014).

[26] J. A. Osborn, Demagnetizing factors of the general ellipsoid, Phys. Rev. **67**, 351 (1945).

[27] S. D. Slöetjes, B. Hjörvarsson, and V. Kapaklis, The effect of confinement on thermal fluctuations in nanomagnets, Appl. Phys. Lett. **118**, 142407 (2021).

[28] S. D. Slöetjes, B. Hjörvarsson, and V. Kapaklis, Texture fluctuations and emergent dynamics in coupled nanomagnets, Phys. Rev. B **106**, 104405 (2022).

[29] A. Vansteenkiste, J. Leliaert, M. Dvornik, M. Helsen, F. Garcia-Sanchez, and B. Van Waeyenberge, The design and verification of MuMax3, AIP Adv. **4**, 107133 (2014).

[30] A. Tryggvason, A. Caruana, C. Kinane, S. Ingvarsson, and F. Magnus, Magnetization dynamics and proximity effects in ultrasoft composition modulated amorphous CoAlZr alloy thin films, Sci. Rep. **15**, 7388 (2025).

[31] K. A. Thórarinsdóttir, N. Strandqvist, V. V. Sigurjónsdóttir, E. B. Thorsteinsson, B. Hjörvarsson, and F. Magnus, Finding order in disorder: Magnetic coupling distributions and competing anisotropies in an amorphous metal alloy, APL Mater. **10**, 041103 (2022).

[32] P. F. Bessarab, V. M. Uzdin, and H. Jónsson, Method for finding mechanism and activation energy of magnetic transitions, applied to skyrmion and antivortex annihilation, Comput. Phys. Commun. **196**, 335 (2015).

[33] P. F. Bessarab, Comment on "Path to collapse for an isolated Néel skyrmion", Phys. Rev. B **95**, 136401 (2017).

[34] V. M. Kuchkin, GNEB in MuMax3, https://kuchkin.github.io/gneb.html.

[35] V. M. Kuchkin and N. S. Kiselev, Homotopy transitions and 3D magnetic solitons, APL Mater. **10**, 071102 (2022).

[36] V. M. Kuchkin, P. F. Bessarab, and N. S. Kiselev, Thermal generation of droplet soliton in chiral magnet, Phys. Rev. B **105**, 184403 (2022).

[37] V. M. Kuchkin, N. S. Kiselev, F. N. Rybakov, I. S. Lobanov, S. Blügel, and V. M. Uzdin, Heliknoton in a film of cubic chiral magnet, Front. Phys. **11**, 1201018 (2023).

[38] M. Sallermann, H. Jónsson, and S. Blügel, Stability of hopfions in bulk magnets with competing exchange interactions, Phys. Rev. B **107**, 104404 (2023).

[39] A. S. Savchenko, V. M. Kuchkin, F. N. Rybakov, and N. S. Kiselev, Magnetic bubbles with alternating chirality in domain walls, Front. Phys. **11**, 1223609 (2023).

[40] P. F. Bessarab, V. M. Uzdin, and H. Jónsson, Harmonic transition-state theory of thermal spin transitions, Phys. Rev. B **85**, 184409 (2012).

[41] P. F. Bessarab, V. M. Uzdin, and H. Jónsson, Potential energy surfaces and rates of spin transitions, Z. Phys. Chem. **227**, 1543 (2013).

[42] V. M. Kuchkin, N. S. Kiselev, F. N. Rybakov, and P. F. Bessarab, Tailed skyrmions—An obscure branch of magnetic solitons, Front. Phys. **11**, 1171079 (2023).

[43] G. D. Chaves-O'Flynn, A. D. Kent, and D. L. Stein, Micromagnetic study of magnetization reversal in ferromagnetic nanorings, Phys. Rev. B **79**, 184421 (2009).